IVYSPRING INTERNATIONAL PUBLISHER

Theranostics

2018; 8(20): 5610-5624. doi: 10.7150/thno.27559

Research Paper

Longitudinal intravital imaging of transplanted mesenchymal stem cells elucidates their functional integration and therapeutic potency in an animal model of interstitial cystitis/bladder pain syndrome

Chae-Min Ryu[1,2*], Hwan Yeul Yu[1,2*], Hye-Yeon Lee[2,3*], Jung-Hyun Shin[1], Seungun Lee[2,3], Hyein Ju[2,3], Bjorn Paulson[4,5], Sanghwa Lee[5,6], Sujin Kim[2,3], Jisun Lim[2,3], Jinbeom Heo[2,3], Ki-Sung Hong[7], Hyung-Min Chung[7,8], Jun Ki Kim[5,6]✉, Dong-Myung Shin[2,3]✉, Myung-Soo Choo[1]✉

1. Department of Urology, Asan Medical Center, University of Ulsan College of Medicine, Seoul, Korea
2. Department of Biomedical Sciences, Asan Medical Center, University of Ulsan College of Medicine, Seoul, Korea
3. Department of Physiology, Asan Medical Center, University of Ulsan College of Medicine, Seoul, Korea
4. Department of Physics, Yonsei University, Seoul, Korea
5. Biomedical Engineering Research Center, ASAN Institute for Life Sciences, Asan Medical Center, University of Ulsan, College of Medicine, Seoul, Korea
6. Department of Convergence Medicine, University of Ulsan, College of Medicine, Seoul, Korea
7. Department of Stem Cell Biology, School of Medicine, Konkuk University, Seoul, Korea
8. Mirae Cell Bio Co. Ltd, Seoul, Korea

*These authors contributed equally to this work.

✉ Corresponding authors: Myung-Soo Choo, MD, PhD, Department of Urology, Asan Medical Center, University of Ulsan College of Medicine, 88 Olympic-ro 43-gil, Songpa-gu, Seoul 05505, Korea. Tel: 82-2-3010-3735; Fax: 82-2-477-8928; E-mail: mschoo@amc.seoul.kr Dong-Myung Shin, Ph.D., Department of Biomedical Sciences, Asan Medical Center, University of Ulsan College of Medicine, 88 Olympic-ro 43-gil, Songpa-gu, Seoul 05505, Korea. Tel: 82-2-3010-2086; Fax: 82-2-3010-8493; E-mail: d0shin03@amc.seoul.kr Jun Ki Kim, Ph.D., Biomedical Engineering Center, ASAN Institute for Life Sciences, Asan Medical Center, Pungnap-2 dong, Songpa-gu, Seoul, 05505, Korea. Tel: 82-2-3010-8497; Fax: 82-2-3010-8493; E-mail: kim@amc.seoul.kr

Received: 2018.05.30; Accepted: 2018.10.08; Published: 2018.11.09

Abstract

Rationale: Mesenchymal stem cell (MSC) therapy may be a novel approach to improve interstitial cystitis/bladder pain syndrome (IC/BPS), an intractable disease characterized by severe pelvic pain and urinary frequency. Unfortunately, the properties of transplanted stem cells have not been directly analyzed *in vivo*, which hampers elucidation of the therapeutic mechanisms of these cells and optimization of transplantation protocols. Here, we monitored the behaviors of multipotent stem cells (M-MSCs) derived from human embryonic stem cells (hESCs) in real time using a novel combination of *in vivo* confocal endoscopic and microscopic imaging and demonstrated their improved therapeutic potency in a chronic IC/BPS animal model.

Methods: Ten-week-old female Sprague-Dawley rats were instilled with 10 mg of protamine sulfate followed by 750 μg of lipopolysaccharide weekly for 5 weeks. The sham group was instilled with phosphate-buffered saline (PBS). Thereafter, the indicated dose (0.1, 0.25, 0.5, and 1×10^6 cells) of M-MSCs or PBS was injected once into the outer layer of the bladder. The distribution, perivascular integration, and therapeutic effects of M-MSCs were monitored by *in vivo* endoscopic and confocal microscopic imaging, awake cystometry, and histological and gene expression analyses.

Results: A novel combination of longitudinal intravital confocal fluorescence imaging and microcystoscopy in living animals, together with immunofluorescence analysis of bladder tissues, demonstrated that transplanted M-MSCs engrafted following differentiation into multiple cell types and gradually integrated into a perivascular-like structure until 30 days after transplantation. The beneficial effects of transplanted M-MSCs on bladder voiding function and the pathological characteristics of the bladder were efficient and long-lasting due to the stable engraftment of these cells.

Conclusion: This longitudinal bioimaging study of transplanted hESC-derived M-MSCs in living animals reveals their long-term functional integration, which underlies the improved therapeutic effects of these cells on IC/BPS.

Key words: Intravital imaging, Multipotent stem cell, Mesenchymal stem cell, Embryonic stem cell, Interstitial cystitis/bladder pain syndrome.

Introduction

The results of preclinical and clinical trials suggest that mesenchymal stem cells (MSCs) are a practical and safe therapeutic option for various human diseases [1-3]. MSCs are multipotent progenitor cells that can be isolated from a wide range of adult sources, such as bone marrow (BM), adipose tissue, peripheral blood, and dental pulp, as well as from fetal sources, such as umbilical cord blood (UCB), Wharton's jelly, placenta, and amniotic fluid [2, 4]. MSCs were recently established by well-controlled differentiation of pluripotent stem cells (PSCs), such as embryonic stem cells (ESCs) and induced PSCs, which can differentiate into all cell types in the body [5, 6]. These PSC-derived cells exhibit several typical features of MSCs and have a better therapeutic potency [7, 8] and *in vivo* engraftment efficacy than those derived from adult tissues [8]. MSCs replace damaged cells in injured tissues, elicit immunomodulatory effects, supply growth factors, mediate cell–cell interactions, and produce matrix proteins that modulate the microenvironment of damaged tissues [9]. Consequently, MSC-based therapies may be useful in regenerative medicine to treat various intractable cardiovascular, musculoskeletal, neurological, and immunological disorders [1-3] as well as several bladder disorders [10].

The bladder disorder interstitial cystitis/bladder pain syndrome (IC/BPS) is likely amenable to stem cell therapy [11]. IC/BPS is a chronic inflammatory condition that affects the submucosal and muscular layers of the bladder [12]. Patients with this condition experience a vague pelvic pain that can be exacerbated by bladder filling and is often associated with urinary frequency, urinary urgency, and decreased quality of life. However, the causes of IC/BPS are unknown and there is no effective treatment or cure [13]. We recently demonstrated that transplantation of MSCs derived from human UCB is a potential therapeutic option for intractable bladder disorders [14, 15]. However, further studies are required regarding the functional integration of MSCs into existing tissues and why these cells engraft poorly *in vivo*.

The therapeutic mechanisms of MSCs remain controversial, which had led to concerns about their therapeutic use [16, 17]. More importantly, the biological and molecular properties of engrafted MSCs in pathological environments have not been directly assessed for the majority of current MSC-based therapies. Consequently, the therapeutic mechanisms of MSCs and the risk of tumorigenesis are uncertain and optimal transplantation protocols have not been established. This has hindered the development of effective and safe MSC-based therapies.

Intravital fluorescence microscopy can be used to study various cellular processes *in vivo*, such as cell trafficking, intercellular interactions, and vascular changes [18]. Dynamic changes in transplanted stem cells can be visualized at the single-cell level using a combination of longitudinal high-resolution confocal imaging and endoscopy. We recently showed that multipotent MSCs (M-MSCs) derived from human ESCs (hESCs) stably integrate into bladder tissues in a hydrochloric acid (HCl) instillation-induced animal model of IC/BPS, which mimics acute urothelial injury [8]. In this previous study, we monitored the distributions and properties of transplanted M-MSCs at single-cell resolution in living animals over 6 months by performing longitudinal intravital confocal imaging of bladder tissues.

In the present study, we applied this novel imaging approach to determine the distribution of transplanted M-MSCs in a lipopolysaccharide (LPS) instillation-induced rat model of IC/BPS, which mimics chronic bladder injury. This demonstrated that M-MSCs migrated from the serosa to the damaged urothelium over 40 days. In addition, immunostaining of tissues showed that M-MSCs differentiated into epithelial, stromal, and endothelial cells, and functionally integrated into pre-existing perivascular cell clusters. Cystometric evaluation of bladder functions in non-anesthetized animals and related mechanistic studies demonstrated that features of chronically damaged bladder tissues, such as non-voiding contraction (NVC), urothelial denudation, and mast cell infiltration, were significantly improved following a single transplantation of a small number of M-MSCs. These data build upon previous studies and demonstrate that hESC-derived M-MSCs are a cost-effective source of therapeutic cells with improved functional integration and potency and are an ideal therapeutic

option for IC/BPS.

Results

Intravital confocal and endoscopic imaging of transplanted M-MSCs in an animal model of IC/BPS

The unlimited proliferation capacity and pluripotency of hESCs may enable production of a large number of high-quality therapeutic cells by well-controlled differentiation *in vitro* and they exhibit improved survival, engraftment, and functionality *in vivo* [7]. We previously reported that hESC-derived M-MSCs remain engrafted in an HCl instillation-induced animal model of IC/BPS until 6 months post-transplantation [8]. However, this model, in which acute pathology is induced by a supra-physiological insult, does not accurately reflect the chronic nature of IC/BPS and consequently its clinical relevance is limited. Here, we used an endotoxin instillation-induced model of chronic bladder pain. Protamine sulfate (PS) and LPS were instilled into the bladders of rats weekly for 5 weeks to induce longer-lasting and chronic urothelial injury, which accurately mimics the chronic and inflammatory nature of IC/BPS [19, 20]. We transplanted the same lot of hESC-derived M-MSCs as was previously transplanted into our acute IC/BPS animal model [8]. In line with this previous report, these cells exhibited several typical features of MSCs, including a spindle- and fibroblast-like morphology (**Figure S1A**) and positive surface expression of markers of MSCs (CD44, CD73, and CD105) and pericytes (CD146 and NG2) (**Figure S1B**). One week after the final instillation, 1×10^6 M-MSCs expressing green fluorescent protein (GFP) were injected directly through the outer layer of the bladder into the area between the muscle and serosa (**Figure 1A**). Lentiviral delivery of a GFP-expressing cassette ensured that the majority of M-MSCs stably expressed GFP during long-term maintenance for up to 5 weeks (**Figure S2A, S2B**) and upon multi-lineage (adipogenic, osteogenic, and chondrogenic) differentiation (**Figure S2C**).

Next, we investigated the properties of engrafted M-MSCs in living animals. To this end, we performed confocal imaging of the outer layers of the bladder close to the injection site by making a small incision in the abdomen (**Figure 1B, 1C**). Meanwhile, we imaged the bladder interior using miniaturized front-view gradient-index (GRIN) endoscopic optical probes, which allowed non-invasive monitoring of the integration of transplanted M-MSCs into the damaged urothelium (**Figure 1B, 1C**). Fluorescence micro-endoscopy of the urothelium and confocal microscopy of the serosa are shown in **Figure 2** and **Figure 3**, respectively. Intense focal fluorescence was detected in the urothelium by endoscopy at 3 days after transplantation (DAT) (**Figure 2**). The fluorescence intensity decreased until 7 DAT, did not change until 14 DAT, increased until 21 DAT, and started to decrease again at around 30 DAT (**Figure S3**). The focus of the images improved over the first 7 DAT and progressively worsened from 30 DAT, indicating that M-MSCs migrated away from the focal plane of the probes. The focal depth of GRIN fluorescence endomicroscopy probes is 20–40 μm in tissues. Therefore, these observations provide physical evidence of cell migration from the serosa and muscularis to the urothelium, followed by cell migration to the lamina propria and differentiation.

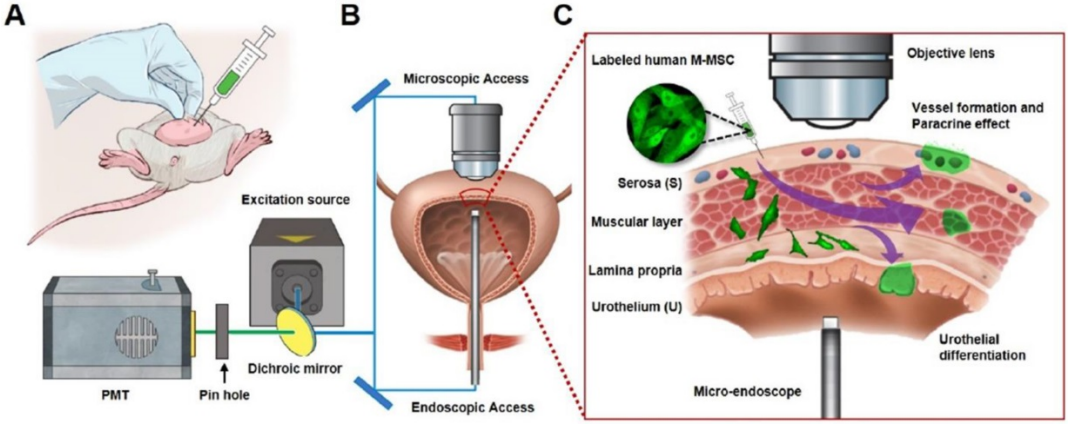

Figure 1. Longitudinal imaging of transplanted M-MSCs in living animals. (A) Schematic diagram of the injection of hESC-derived M-MSCs into the bladder wall of IC/BPS rats. **(B)** Schematic diagram of confocal imaging of the external bladder wall and micro-endoscopy of the internal bladder wall to monitor the distribution, migration, and integration of transplanted M-MSCs. The objective lens was inserted through a small incision in the overlying abdomen to image the outer layer of the bladder. The front-view GRIN micro-endoscope probe was inserted into the bladder of an anesthetized rat on an XYZ stage to image the surface of the urothelium. **(C)** Schematic diagram of the migration of M-MSCs from the serosa, where they were injected, to the lamina propria and urothelium. M-MSCs initially differentiate in the urothelium and thereby repair the denuded urothelial wall, and later integrate into blood vessel-like structures. The injection site of M-MSCs and the viewpoints are indicated.

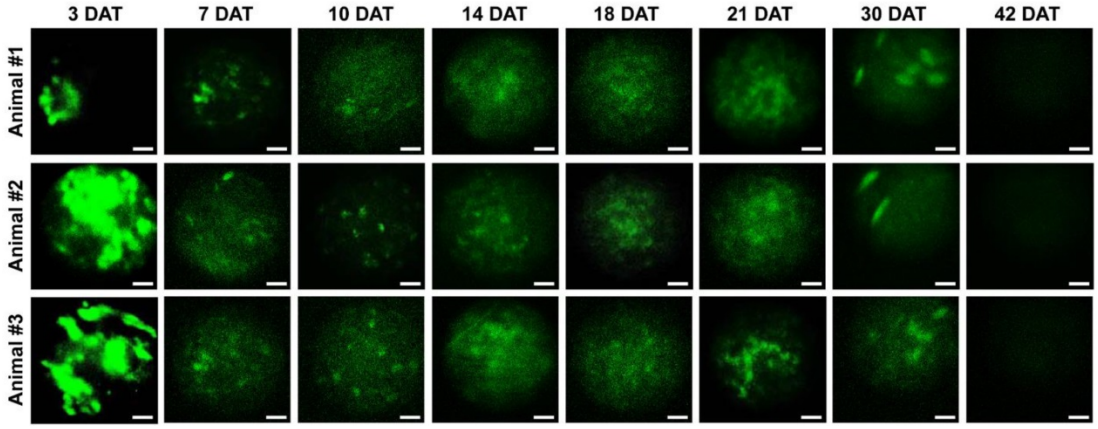

Figure 2. Longitudinal microcystoscopy of transplanted M-MSCs in living animals. Time-lapse micro-endoscopy imaging of engrafted M-MSCs in the bladders of LPS-IC rats (three independent animals) at 3–42 days after transplantation (DAT). Endoscopic images obtained using a GRIN optical probe (magnification ×40, scale bar = 50 μm). Quantitative data of intravital micro-endoscopic imaging is presented in **Figure S3**. Representative movies obtained from these experiments are available as **Supplementary Movies**.

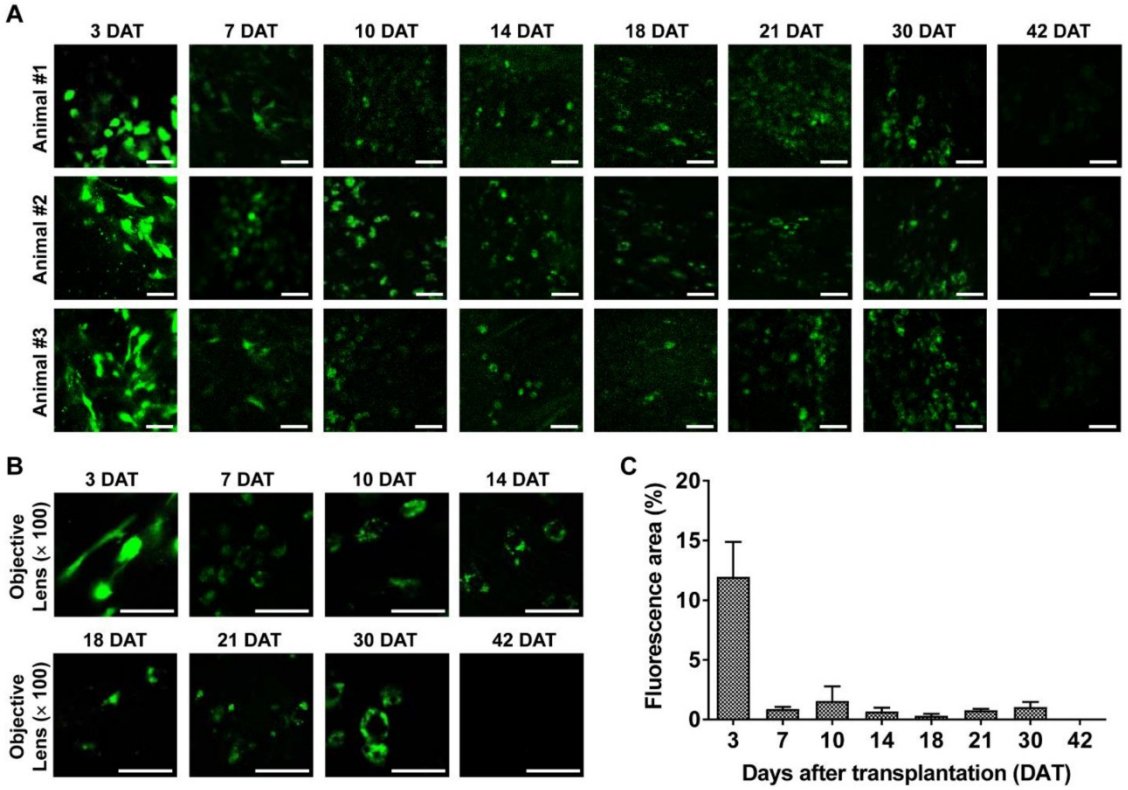

Figure 3. Longitudinal confocal microscopy of transplanted M-MSCs in living animals. Time-lapse confocal microscopy of engrafted M-MSCs in the bladders of LPS-IC rats (three independent animals) at 3–42 days after transplantation (DAT). **(A and B)** Confocal micrographs obtained using an objective lens (**A**; magnification ×40, scale bar = 50 μm and **B**; ×100, scale bar = 50 μm). The majority of transplanted M-MSCs at 30 DAT were detected in a vascular-like structure located close to the outer layer of the bladder. **(C)** Percentage of the fluorescent area in confocal micrographs. Representative movies obtained in these experiments are available as **Supplementary Movies**.

Intravital confocal imaging of the outer layers of the bladder yielded similar findings. The fluorescence intensity decreased rapidly until 7 DAT and gradually until 42 DAT (**Figure 3**). The GFP$^+$ cells had multiple shapes and were distributed throughout the entire bladder at 3 DAT. GFP fluorescence at 3 DAT, which labeled cells with multiple shapes and was broadly distributed across the entire bladder, was observed in both endoscopy (**Figure 2**) and confocal micrographs (**Figure 3A, 3B**). As the fluorescence intensity decreased from 7 DAT (**Figure 3C**), engrafted GFP$^+$ cells came into focus and the majority were located in blood vessel-like structures in confocal micrographs (**Figure 3A, 3B**). Negligible baseline fluorescence or autofluorescence was detected in animals not injected with GFP$^+$ M-MSCs (**Figure S4A, S4B**). Little GFP

fluorescence with clear cellular morphology was observed at 42 DAT.

Immunostaining of transplanted M-MSCs in an animal model of IC/BPS

Exposure to dramatic environmental changes or adverse microenvironments in damaged tissues may induce apoptosis of transplanted MSCs and impair their engraftment. Terminal deoxynucleotidyl transferase dUTP nick-end labeling (TUNEL) of bladder tissues indicated that apoptosis of transplanted GFP$^+$ M-MSCs was highest at 3 DAT, at which point ~20% of these cells were apoptotic (**Figure S5**). The percentage of transplanted cells that were apoptotic was reduced to less than 10% at 7 DAT, and almost none of these cells were apoptotic at 30 DAT. These findings indicate that apoptosis also contributes to the rapid decline in GFP fluorescence up to 3 DAT in both endoscopy (**Figure 2**) and confocal micrographs (**Figure 3**).

Next, to analyze the cellular properties of surviving M-MSCs, immunohistological analysis of bladder tissues was performed by multichannel scanning laser confocal imaging. Engrafted cells, epithelial cells, stromal cells, and endothelial cells were detected based on expression of GFP, E-cadherin, vimentin, and CD31, respectively (**Figure 4, Figure S6,** and **Figure S7**). At 7 DAT, many GFP$^+$ cells were detected in the urothelium, lamina propria, and serosa. The majority of these cells were located between the serosa and muscular layer, where they had been injected, and a few were found in the muscular layer. All GFP$^+$ cells in the urothelium were E-cadherin$^+$, indicating that they had differentiated into epithelial cells (**Figure 4A, top row**). The majority of GFP$^+$ cells located between the serosa and muscularis were strongly stained with an anti-vimentin antibody, indicating that they had differentiated into stromal cells (**Figure 4A, second row**) and perivascular cells (**Figure 4A, third row**). GFP$^+$ cells located in the endothelium were CD31$^+$, indicating that they had differentiated into endothelial cells (**Figure 4A, fourth row**). Non-specific staining in immunofluorescence assays was ruled out by two negative controls: i) co-staining with mouse and rabbit IgG control antibodies instead of primary antibodies, and ii) co-staining of bladder sections from animals not injected with GFP$^+$ M-MSCs (**Figure S6A**). Taken together, these results demonstrate that transplanted M-MSCs stably engrafted and migrated to the damaged urothelium, where they differentiated into multiple cell types.

Consistent with the intravital imaging, GFP$^+$ cells in the urothelium were rarely observed from 30 DAT and mainly localized in the serosa (**Figure 4B**). During this period, engrafted cells formed discrete foci and the majority were detected in blood vessel-like structures. Confocal imaging of bladder tissues indicated that engrafted M-MSCs had differentiated into CD31$^+$ endothelial cells as well as vimentin$^+$ or α-smooth muscle actin (SMA)$^+$ perivascular cells close to blood vessels at 30 DAT (**Figure 4B** and **Figure S6B**). The differentiation of transplanted cells into perivascular cells was further evaluated by investigating cells that co-expressed vimentin and human β2 microglobin (hB2M) in blood vessel-like structures (**Figure S7**). However, no such cells were observed at 42 DAT (**Figure S8**). In summary, by performing a combination of intravital imaging and immunohistological analysis, we monitored and characterized M-MSCs engrafted in the bladder of a rat model of IC/BPS as they initially replenished the urothelial layer and progressively differentiated into perivascular cells.

Evaluation of the therapeutic potency of M-MSCs in an animal model of IC/BPS

M-MSCs stably engrafted for more than 1 month. Therefore, we next investigated the therapeutic effects elicited following a single administration of 1×10^6 M-MSC directly into the bladders of rats with LPS-induced IC/BPS (LPS-IC rats). To precisely investigate functional improvement, we performed awake filling cystometry, which allows long-term evaluation of bladder voiding function in free-moving animals (Figure 5A, 5B). LPS-IC rats exhibited irregular voiding patterns, and the micturition interval (MI; 27.42±0.55 vs. 98.29±1.56 sec; $p<0.001$), micturition volume (MV; 0.15±0.01 vs. 0.35±0.02 mL; $p<0.001$), bladder capacity (BC; 0.18±0.00 vs. 0.66±0.01 mL; $p<0.001$), and residual volume (RV; 0.03±0.01 vs. 0.31±0.02 mL; $p<0.005$) were lower in these rats than in sham-operated rats (Figure 5B, 5C). Micturition pressure (MP; 95.86±1.45 vs. 53.29±0.45 cmH_2O; $p<0.001$), basal bladder pressure (BP) (60.95±4.12 vs. 31±2.3 cmH_2O; $p<0.01$), and maximum BP (97.17±1.45 vs. 53.43±0.45 cmH_2O; $p<0.001$) were higher in LPS-IC rats than in sham-operated rats.

A single transplantation of 1×10^6 M-MSCs into rats with LPS-induced IC/BPS (LPS-IC + M-MSC rats) significantly improved these voiding parameters (**Figure 5B, 5C**). Beneficial effects were also observed upon administration of as few as 2.5×10^5 M-MSCs (**Figure 5B, 5C**). In particular, the frequency of contraction during the non-voiding period (NVC), which is the parameter most commonly used to evaluate bladder voiding function in clinical settings, was significantly ameliorated in LPS-IC + M-MSC rats compared with LPS-IC rats.

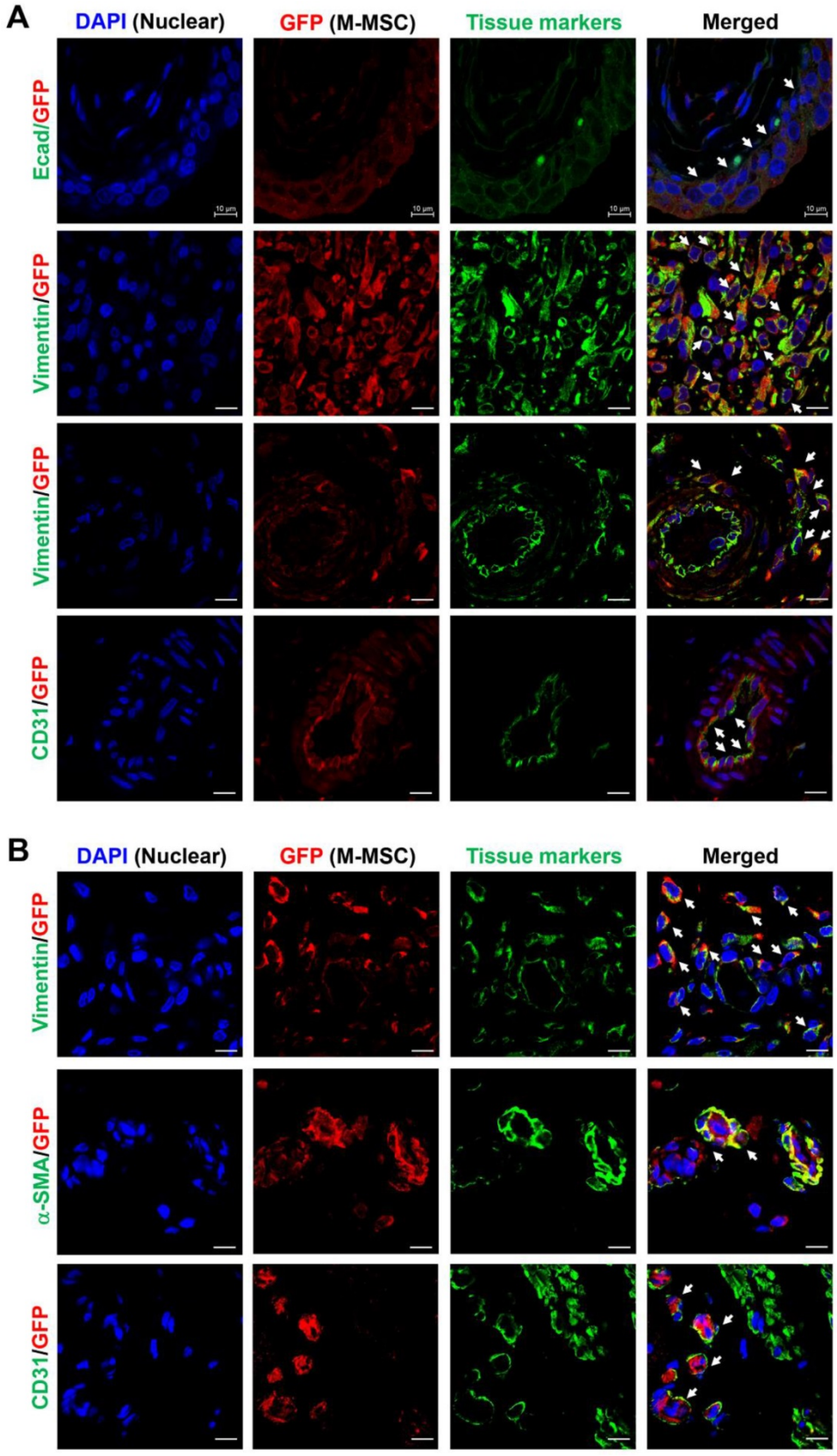

Figure 4. Immunostaining analysis of transplanted M-MSCs. Confocal micrographs of M-MSCs stably expressing GFP (red) and immunostaining of the marker proteins E-cadherin (Ecad), vimentin, α-SMA, and CD31 (green) in bladder sections of LPS-IC + M-MSC rats at 7 DAT **(A)** and 30 DAT **(B)** (magnification ×1,000, scale bar = 10 μm). Nuclei were stained with DAPI (blue). Arrows indicate GFP$^+$ engrafted cells co-expressing each tissue marker. Notably, the majority of transplanted GFP$^+$ cells at 7 DAT was strongly stained with the vimentin expressing stromal cells (**second row in A**) and perivascular cells (**third row in A**).

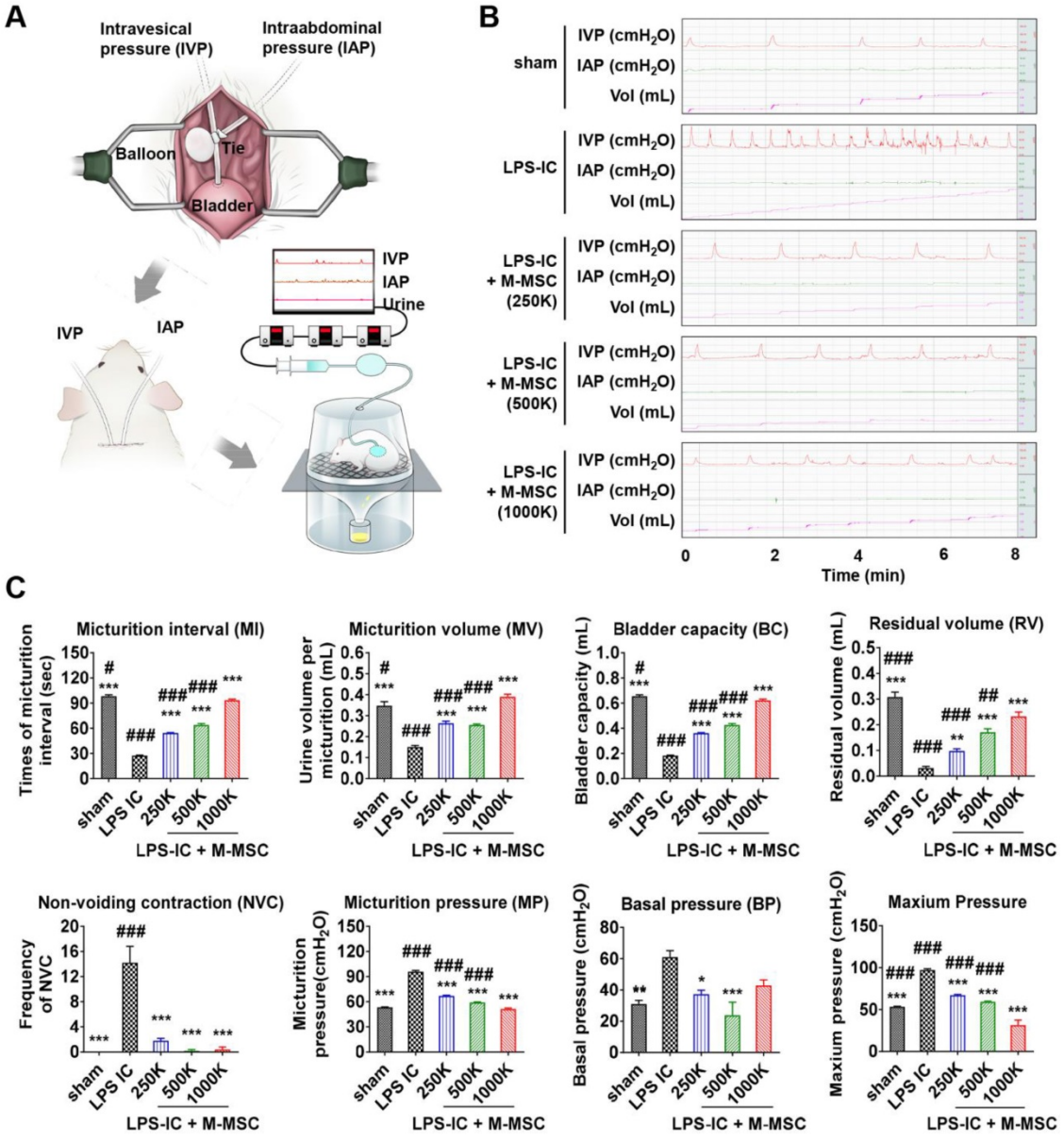

Figure 5. Injection of M-MSCs ameliorates bladder voiding functions in LPS-IC rats. (A) Schematic diagram of awake cystometry. **(B and C)** Representative awake cystometry results **(B)** and quantitative bladder voiding data **(C)** at 1 week after injection of LPS-IC rats with the indicated number of M-MSCs (K = thousand). Data are presented as the mean ± SEM (five independent animals per group). *p<0.05, **p<0.01, and ***p<0.001 compared with the LPS-IC group; #p<0.05, ##p<0.001, and ###p<0.001 compared with the 1000 K group according to a one-way ANOVA with the Bonferroni post-hoc test. Sham: sham-operated.

Consistent with awake cystometry data, administration of more than 2.5×10^5 M-MSCs restored histological alterations in LPS-IC rats, such as severe urothelial denudation, mast cell infiltration, and an increase in apoptosis (**Figure 6A, 6B**). Tissue fibrosis was slightly increased in the bladders of LPS-IC rats and was repaired by a single transplantation of a low number of M-MSCs.

Next, we examined whether LPS-IC rats exhibited chronic symptoms, similar to IC/BPS patients. These animals exhibited defective bladder voiding functions for up to 4 weeks after the final LPS instillation (**Figure 7A** and **Figure S9**). Accordingly, increases in urothelial denudation, inflammation, mast cell infiltration, and apoptosis, which are typically observed in the bladders of IC/BPS patients [21-24], were sustained for more than 4 weeks in the bladder tissues of LPS-IC rats (**Figure 7B, 7C,** and **Figure S10**). The therapeutic effects of a single administration of M-MSCs on bladder voiding functions and histological injuries were sustained for 2–4 weeks after transplantation (**Figure 7**). In particular, normal NVC was observed in LPS-IC + M-MSC rats for up to 4 weeks after transplantation of M-MSCs (**Figure 7A**). This preclinical study demonstrates that transplantation of M-MSCs

effectively improves voiding functions and histological damage typically observed in the bladders of IC/BPS patients and prevents further tissue damage.

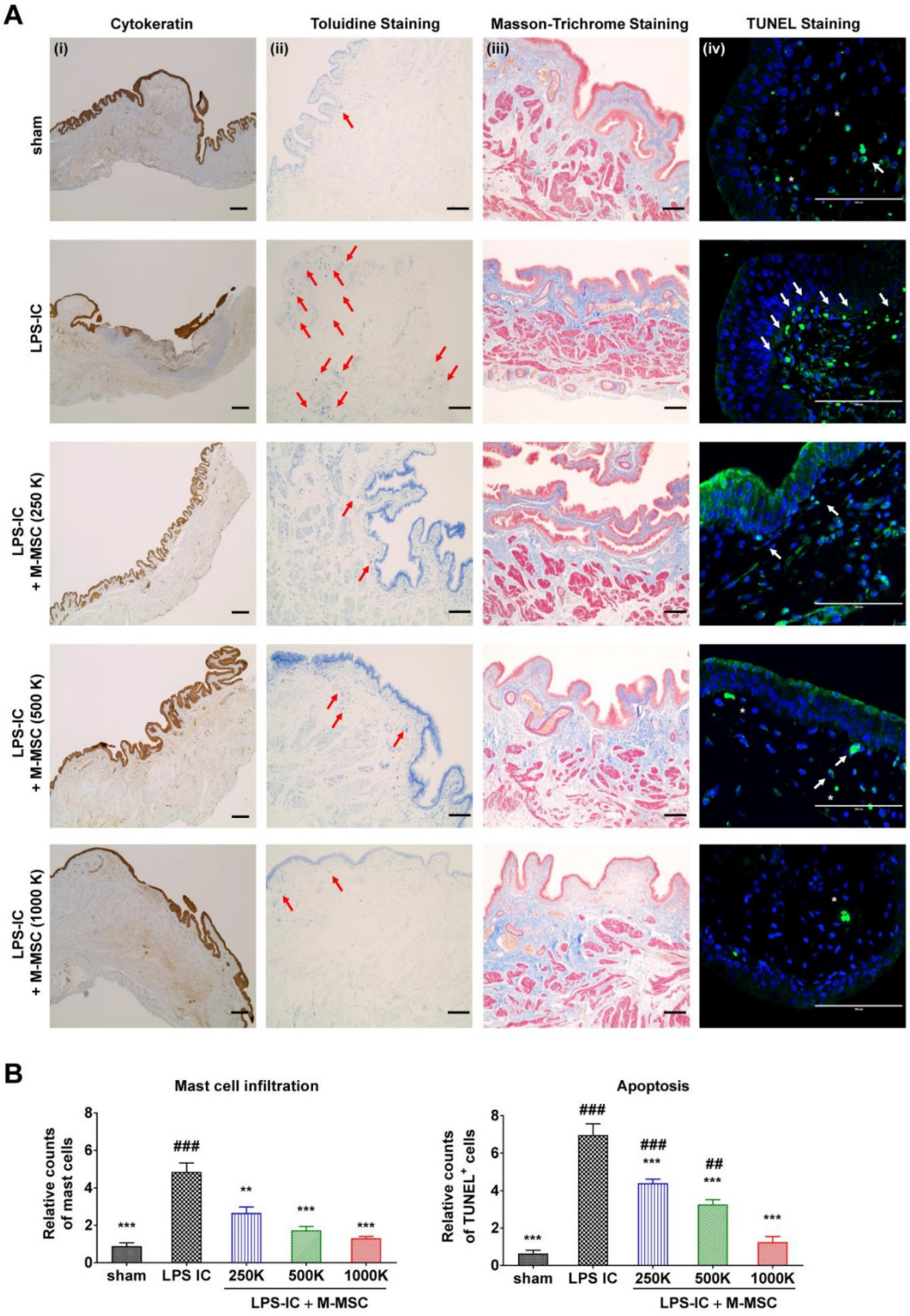

Figure 6. Injection of M-MSCs ameliorates histological abnormalities in the bladders of LPS-IC rats. (A) (i) Cytokeratin immunostaining (magnification ×40, scale bar = 200 μm), (ii) Toluidine blue staining (magnification ×100, scale bar = 200 μm), (iii) Masson's trichrome staining (magnification ×100, scale bar = 200 μm), and (iv) TUNEL (magnification ×400, scale bar = 100 μm) of bladder tissues of LPS-IC rats at 1 week after injection of the indicated number of M-MSCs (K = a thousand) or PBS. Arrows indicate infiltrated mast cells (ii) or apoptotic cells (iv). Sham: sham-operated. **(B)** Quantification of histological staining. Three representative areas per slide were randomly selected from five independent animals. Data (n = 15) were normalized against those in sham-operated rats and are presented as the mean ± SEM. **p<0.01 and ***p<0.001 compared with the LPS-IC group; #p<0.05, ##p<0.001, and ###p<0.001 compared with the 1000 K group according to a one-way ANOVA with the Bonferroni post-hoc test.

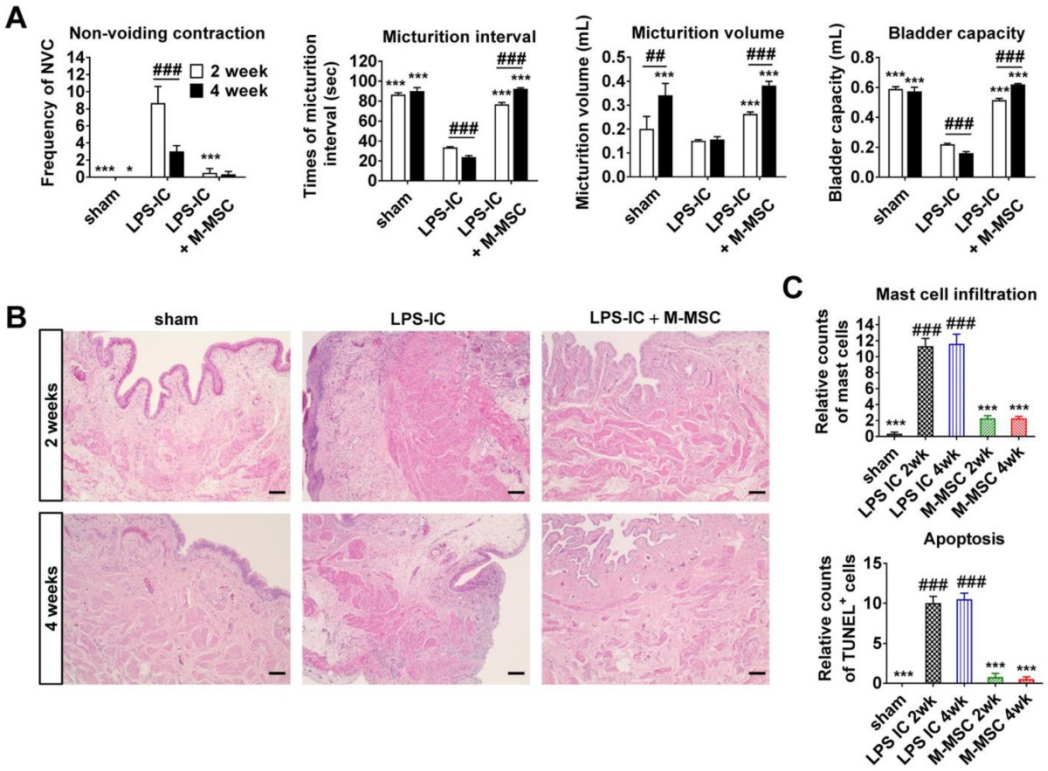

Figure 7. Long-term therapeutic effects of M-MSCs in LPS-IC rats. (A) Quantitative bladder voiding data in LPS-IC rats at 2 and 4 weeks after injection of 1×10^6 M-MSCs. Data are presented as the mean ± SEM (six independent animals per group). **p<0.01 and ***p<0.001 compared with the LPS-IC group; ###p<0.001 for 2 weeks vs. 4 weeks according to a two-way ANOVA with the Bonferroni post-hoc test. NAC; non-voiding contraction. **(B)** Hematoxylin and eosin staining of the indicated bladder tissues (magnification ×200, scale bar = 200 μm). Nuclei were stained with Mayer's hematoxylin. **(C)** Quantification of mast cell infiltration and apoptosis in bladder tissues of LPS-IC rats at 2 and 4 weeks after injection of 1×10^6 M-MSCs. Three representative areas per slide were randomly selected from five independent animals. Data (n = 15) were normalized against levels in sham-operated rats and are presented as the mean ± SEM. ***p<0.001 compared with the LPS-IC group; ###p<0.001 compared with the LPS-IC + M-MSC group according to a one-way ANOVA with the Bonferroni post-hoc test.

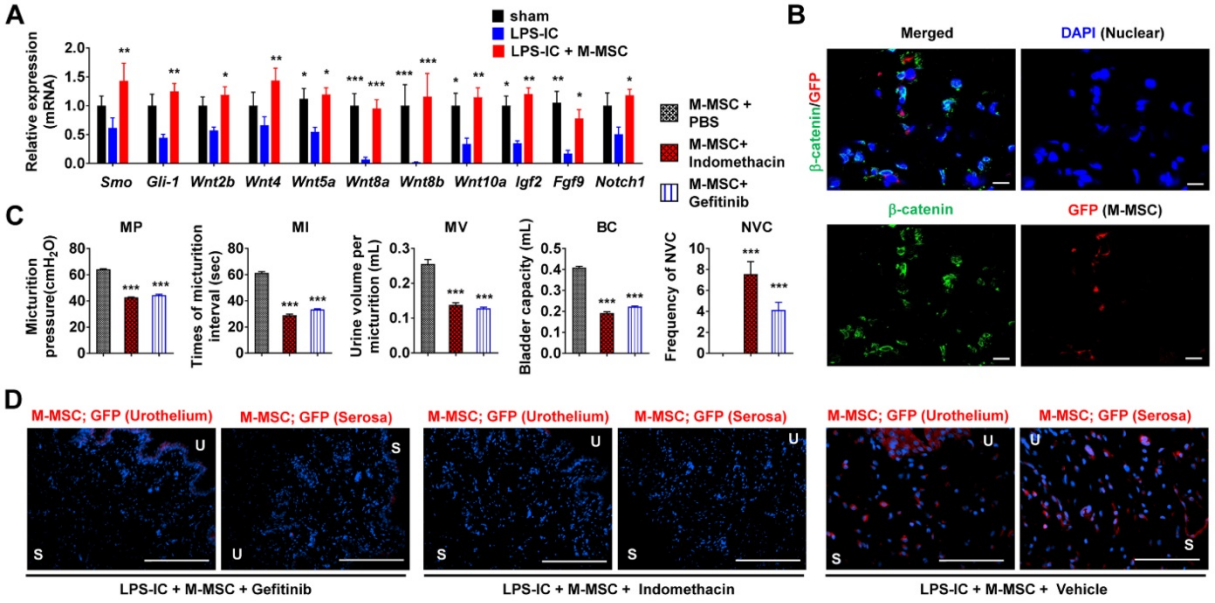

Figure 8. Role of WNT signaling in the therapeutic effects of M-MSCs. (A) RQ-PCR analyses of the expression levels of *Shh*, *WNT*, and downstream growth factors in the bladder tissues of LPS-IC rats at 1 week after injection of 1×10^6 M-MSCs or PBS. RQ-PCR assays were performed in duplicates for five independent animals. Expression levels (n = 10) were normalized against those in sham-operated rats and are presented as the mean ± SEM. *p<0.05, **p<0.01, and ***p<0.001 compared with the LPS-IC group according to a two-way ANOVA. **(B)** Representative confocal micrographs (magnification ×1,000, scale bar = 10 μm) of bladder sections of LPS-IC rats transplanted with GFP+ M-MSCs. Samples were co-stained for GFP (red) and β-catenin (green). Nuclei were stained with DAPI (blue). **(C)** Quantitative bladder voiding data in LPS-IC rats (eight independent animals per group) at 1 week after injection of 1×10^6 M-MSCs in the absence or presence of indomethacin or Gefitinib, which inhibit WNT and IGF-mediated signaling, respectively. All data are presented as the mean ± SEM. ***p<0.001 compared with the LPS-IC group according to a one-way ANOVA with the Bonferroni post-hoc test. **(D)** Immunostaining of M-MSCs stably expressing GFP (red) in the bladders of the indicated rats (magnification ×200, scale bar = 200 μm). U: urothelium; S: serosa; sham: sham-operated.

WNT signaling is involved in the therapeutic effects of M-MSCs

MSC therapy stimulates epithelial regeneration by activating the sonic hedgehog (Shh) and WNT pathways in the HCl instillation-induced animal model of acute IC/BPS [8, 14]. Gene expression of *Smoothened* (*Smo*), a transducer of Shh signaling, WNT family genes (e.g., *Wnt2b*, *Wnt4*, *Wnt5a*, *Wnt8a*, *Wnt8b*, and *Wnt10a*), and their downstream growth factors (e.g., *Igf2*, *Fgf9*, and *Notch1*) was downregulated in bladder tissues of LPS-IC rats (**Figure 8A**). These decreases were significantly ameliorated by M-MSC therapy. Expression and nuclear localization of β-catenin, a surrogate marker of WNT signaling activation, were increased in LPS-IC + M-MSC rats (**Figure 8B** and **Figure S11A, S11B**). The majority of cells containing nuclear β-catenin were located close to GFP^+ cells (**Figure 8B**), suggesting that engrafted M-MSCs established a microenvironment that stimulated WNT signaling.

To validate the significance of WNT signaling and downstream growth factors in the therapeutic effects of M-MSCs, we injected rats daily with indomethacin [25] or Gefitinib [26] to inhibit WNT and IGF-mediated signaling, respectively. Injection of either inhibitor significantly abrogated the therapeutic effects of M-MSCs on bladder voiding functions in LPS-IC rats (**Figure 8C**) and significantly impaired the engraftment of M-MSCs (**Figure 8D** and **Figure S11C**). These results indicate that the WNT and IGF signaling cascades are involved in the therapeutic effects of M-MSCs on chronic inflammatory bladder injuries in IC/BPS.

Discussion

IC/BPS is a heterogeneous and multifactorial disease [27, 28]. Unfortunately, its etiology is not fully understood and there is no cure. Recent studies reported that >2% of females may suffer from IC/BPS, which is much higher than its previously reported prevalence of 0.1% [29]. Although several treatments have been developed, these do not improve the symptoms of many patients, who continue to suffer from sleep disturbance, sexual dysfunction, depression, anxiety, and stress, and thus have a reduced quality of life [30]. Consequently, clinical treatment of IC/BPS remains challenging [31, 32]. The pathogenesis of IC/BPS needs to be investigated and animal models of this disease need to be developed to identify curative treatments. Several pathophysiological features of IC/BPS were recently described, including inflammation and mast cell activation, nitric oxide or an autoimmune mechanism, and a glycosaminoglycan layer defect [33-36]. Stem cells may ameliorate IC/BPS by undergoing differentiation to regenerate the denuded urothelium and by secreting trophic factors to modulate chronic inflammation and immune responses [11].

We previously reported that UCB-derived MSCs elicit beneficial effects on IC/BPS and ketamine-induced cystitis [14, 15]. However, these cells survive for less than 1 week after transplantation and have a limited capacity to integrate into bladder tissues. The therapeutic effects of MSCs without long-term engraftment are explained by paracrine factors, which are growth factors and cytokines secreted by transplanted stem cells that exert cytoprotective, pro-angiogenic, anti-inflammatory, and immunomodulatory effects, rather than by direct repair of damaged tissues [37-39]. However, the details of these paracrine mechanisms remain controversial. Poor understanding of the therapeutic mechanisms and behaviors of transplanted MSCs *in vivo* has led to skepticism about current MSC-based therapies.

In the present study, we transplanted M-MSCs into a rat model of chronic IC/BPS. Therapeutic effects can be assessed for a longer duration and therapeutic mechanisms can be more accurately determined in this reliable animal model. Unlike their adult tissue counterparts, hESC-derived M-MSCs survived for longer than 1 month after transplantation. The enhanced engraftment and survival of M-MSCs underlies their superior and longer-lasting therapeutic potency in this animal model of IC/BPS. Indeed, the therapeutic potency of M-MSCs was superior to that of BM-derived MSCs (BM-MSCs) in LPS-IC rats (**Figure S12A, S12B**). In particular, a sustained therapeutic effect for up to 4 weeks was not observed following a single administration of BM-MSCs (**Figure S12C, S12D**).

In terms of a mechanism of action, the WNT and IGF signaling cascades were involved in the beneficial effects of M-MSCs. Thus, we speculate that engrafted M-MSCs protect the urothelial layer of the bladder against further environmental damage and establish a microenvironment conducive for tissue repair. The high resolution of intravital confocal imaging and microcystoscopy allowed direct observation of the differentiation of M-MSCs into perivascular cells and formation of stable multicellular structures, which may initiate the therapeutic effects.

Objective lenses have previously only been used to image superficial tissues *in vivo*, such as skin or surgically exposed organs, due to their large sizes. Here, we imaged bladder tissues in a minimally invasive manner by performing cystoscopy using a micro-endoscope with a small-diameter GRIN lens. While engrafted cells were only tracked for a limited

period of time by endoscopy, this approach confirmed that M-MSCs migrated to and engrafted in the urothelium and allowed limited visualization of these cells in the lamina propria. The defocusing and decreased fluorescence labeling of cells after 21 DAT were likely due to the limited focal depth of the GRIN lens and the limited optical penetration depth of visible light-based endoscopy, which are both ~100 μm in most soft tissues.

The GRIN lens and confocal objective lens could only image a small area and consequently could not be used to verify that the injected M-MSCs dispersed throughout the entire bladder. However, cystometry revealed that bladder regulation was improved in LPS-IC + M-MSC rats and that the beneficial effects of M-MSCs were not restricted to the site of injection, demonstrating that these cells were not targeted to particular regions of the bladder and affected the entire urothelium. M-MSCs migrated from the bladder serosa, the site at which they were injected, to the severely damaged urothelium over 3 days. This is the first report of the migration of transplanted stem cells in a living animal model of IC/BPS, to the best of our knowledge. Although a considerable percentage of M-MSCs underwent apoptosis soon after transplantation (**Figure S5**), we speculate that the decreases in fluorescence intensity and the number of M-MSCs between 3 and 7 DAT were also attributable to the dispersal of these cells throughout the entire bladder.

Following migration of transplanted M-MSCs from the bladder serosa to the mucosa over 7 days, these cells differentiated into endothelial and epithelial cells in the urothelium, lamina propria, and serosa over 30 days. This correlated with improvements of IC/BPS symptoms, including bladder denudation and NVC, in LPS-IC + M-MSC rats. Transplanted M-MSCs clearly integrated into functional compartments of the bladder and differentiated into E-cadherin$^+$ urothelial cells, CD31$^+$ endothelial cells, and vimentin$^+$ stromal cells and pericytes. In particular, engraftment of cells in the lamina propria and urothelium stimulated WNT-related epithelial regeneration. Thus, functional integration of transplanted M-MSCs might effectively ameliorate chronic inflammatory injury in IC/BPS patients by restoring the urothelial barrier function to prevent urine leakage and by establishing immunomodulatory and anti-inflammatory microenvironments. In a further study, the contributions of these two therapeutic effects (direct differentiation in the damaged urothelium and modulation of the microenvironments) should be carefully scrutinized not only to gain further insight the mechanism of action of M-MSC-based therapy, but also to successfully translate these preclinical data into clinical applications.

In our previous study of an HCl instillation-induced animal model of IC/BPS, engrafted M-MSCs were observed until 6 months post-transplantation [8]. By contrast, engrafted M-MSCs in LPS-IC rats were rarely observed at 6 weeks post-transplantation by intravital imaging (**Figure 2** and **Figure 3**) or immunohistological analysis (**Figure S8**). Differences in tissue microenvironments between these two animal models may affect the engraftment and integration of transplanted M-MSCs. Although immune rejection and tissue inflammation were not observed in the current study, differences in immune responses between the two animal models may underlie differences in the dynamics of the transplanted cells. Due to the immunomodulatory capacities of MSCs derived from several sources, allogeneic and xenogeneic transplantation of these cells has been performed to improve various diseases, and significant therapeutic effects were observed in most cases [40]. Likewise, we previously reported that hESCs and their differentiated progeny show little immunogenic potency because they lowly express immunologically relevant cell surface markers, including HLA-DR and costimulatory molecules (CD40, CD40L, B7-1, and B7-2) [5, 8, 41]. Despite the low immunogenicity of M-MSCs, the immune response to these cells should be thoroughly investigated in a further study.

Stem cell research in urology is rapidly advancing, and consequently stem cell therapies are expected to be clinically applied in the near future [14, 42, 43]. To overcome the limitations of current MSC-based therapies, we suggest that hESC-derived M-MSCs are a cost-effective source of therapeutic cells with an improved functional potency without any adverse tumorigenic or immunogenic outcomes. hESC-derived MSCs possess important advantages, including the capacity to generate an almost unlimited supply of therapeutic cells. By undergoing controlled differentiation, the safety and potency of hESC derived cells are maintained prior to transplantation. Despite these advantages, one major obstacle to the therapeutic application of hESC-derived cells is the risk of tumorigenesis [44]. As previously observed in our acute IC/BPS model [8], adverse effects, including formation of teratomas and other tumors, immune reactions, and differentiation of transplanted M-MSCs into unwanted cell types, were not detected in healthy control rats or those with LPS-induced chronic IC/BPS up to 1 year after transplantation (data not shown). However, the safety issues surrounding

hESC-based therapies must be thoroughly investigated before these cells are clinically applied. In particular, studies are required to investigate how the effects of these cells vary according to whether recipients are immunosuppressed, the interval and frequency of stem cell administration, and the severity or pathophysiology of the disorder [44].

Conclusion

In the present study, using a combination of longitudinal intravital confocal imaging and microcystoscopy, we characterized the distributions, properties, and intercellular interactions of hESC-derived M-MSCs transplanted into an animal model of chronic IC/BPS. We monitored the migration and differentiation of transplanted M-MSCs in the urothelium and demonstrated that the WNT and IGF signaling cascades are involved in the long-term therapeutic effects of these cells. The biological properties of engrafted stem cells, including transcriptional activity, external signal transduction, and differentiation potency, may vary according to the environment [45]. Therefore, the present study reporting longitudinal analysis of engrafted cells in living animals may improve understanding of the cellular mechanisms underlying functional improvement, clarify the risk of tumorigenesis after transplantation, and help to optimize transplantation protocols prior to clinical trials.

Methods

Animal models and administration of M-MSCs

All animal experiments were approved by the Institutional Animal Care and Use Committee of the University of Ulsan College of Medicine (IACUC-2016-12-088). The LPS-IC rat model was established by instilling PS (10 mg/rat; Sigma-Aldrich, St. Louis, MO, USA) into the bladders of 10-week-old female Sprague-Dawley rats (Orient Bio, Gapyong, Gyeonggi-do, Korea) via the urethra using a 26-gauge angiocatheter to denude the urothelium. After 45 min, the bladder was emptied, washed with phosphate-buffered saline (PBS), and treated with LPS (750 μg/rat; Sigma-Aldrich) for 30 min to induce inflammation. Thereafter, PS and LPS were instilled weekly for 5 weeks to induce chronic urothelial injury. One week after the final instillation, a lower abdominal incision was made and the indicated number of hESC-derived M-MSCs or PBS was directly injected into the outer layer of the anterior wall and dome of the bladder using a 300 μL syringe and a 26-gauge needle, as previously reported [8, 14, 15, 46].

Culture of hESC-derived M-MSCs and establishment of GFP$^+$ M-MSCs

H9 hESCs were differentiated into M-MSCs as previously described [5, 7]. Established M-MSCs were cultured in EGM2-MV medium (Lonza, San Diego, CA, USA) on plates coated with rat tail collagen type I (Sigma-Aldrich) in a humidified atmosphere containing 5% CO_2 at 37°C. Surface marker expression and multi-lineage differentiation of M-MSCs were characterized as previously described [8, 47]. All M-MSCs were expanded for fewer than ten passages to ensure they remained multipotent. To stably express GFP, M-MSCs were infected with a GFP-expressing lentivirus, which was generated as previously described [47]. In brief, GFP was sub-cloned into the pENTR4 entry vector (Invitrogen, Carlsbad, CA, USA) and then transferred to the pLenti6.2/V5-DEST lentiviral vector (Invitrogen) using Gateway® Technology (Invitrogen). Lentivirus was produced using a four-plasmid transfection system (Invitrogen). Two days after transfection of the 293 FT packaging cell line, supernatants containing recombinant pseudo-lentiviral particles were collected and concentrated by precipitation using a Lenti-X Concentrator kit (Clontech, Mountain View, CA, USA). M-MSCs were infected with the concentrated virus using 6 μg/mL polybrene (Invitrogen), and infected cells were selected using 6 μg/mL blasticidin (Invitrogen). Stable expression of GFP was examined using a BDFACS Canto II flow cytometer (BD Biosciences, Mountain View, CA, USA) and an inverted fluorescence microscope (EVOS FL Color Imaging System, Life Technologies, Carlsbad, CA, USA).

Longitudinal in vivo confocal imaging and micro-endoscopy

A total of 1×10^6 GFP$^+$ M-MSCs were injected into the bladder serosa of LPS-IC rats, following acquisition of baseline images (**Figure S4B**). Confocal microscopy and imaging with a micro-endoscopic optical probe were performed in living animals before transplantation and for up to 6 months post-transplantation. For confocal microscopy, a 5 mm incision was made in the abdomen and widened to expose the bladder and allow imaging using a 40× objective lenses. The microscope was aligned such that the site of injection was centered, with deviations of less than 1 mm. The excitation laser was focused on the outer layer of the bladder, and then the point of focus was adjusted inward to attain consistent and meaningful image depths. For cystoscopy, a micro-endoscope with a diameter of 1.2 mm and a length of 5.5 cm was fabricated by cementing three GRIN lenses together in a rigid tube suitable for

front-view image transfer [18]. The transverse and lateral resolutions were 1 and 11 μm in air, respectively, which was sufficient to monitor M-MSCs at single-cell resolution in the bladder mucosa. A custom-built system with three axes of translational freedom was used to mount and align the probe consistently in the confocal microscope, and the probe was inserted via the urethra and positioned close to the pelvis. Care was taken to ensure that the procedure and alignment were performed consistently, resulting in deviations of less than 0.5 mm. Focus was attained by abutting the GRIN probe to the inner bladder wall and adjusting the point of focus inward using the microscopy platform. GFP was excited using a continuous 488 nm laser diode and was scanned along the objective and endoscope tip at a rate of 30 fps using a scanning galvanometric system. Photomultiplicative detectors were used in tandem with dichroic filters to capture emitted fluorescence while avoiding noise caused by the excitation laser and autofluorescence.

Unanesthetized and unrestrained cystometry (awake cystometry)

Cystometric evaluation was performed in awake and unrestrained animals in metabolic cages. Three days prior to the cystometrogram, intravesical pressure (IVP) and intra-abdominal pressure (IAP) were measured, as described previously [48, 49]. The urethra was approached using a PE-50 catheter (Clay Adams, Parsippany, NJ) connected to a pressure transducer (Research Grade Blood Pressure Transducer; Harvard Apparatus, Holliston, MA, USA) and a microinjection pump (PHD22/2000 pump; Harvard Apparatus). The voiding volumes were recorded using a fluid collector connected to a force displacement transducer (Research Grade Isometric Transducer; Harvard Apparatus) as normal saline was infused into the bladder at a rate of 0.4 mL/min. The IVP, IAP, and voiding volumes were recorded continuously using Acq Knowledge 3.8.1 software and an MP150 data acquisition system (Biopac Systems, Goleta, CA, USA) at a sampling rate of 50 Hz. Mean values were calculated from three reproducible voiding cycles in individual animals. NVC was defined when IVP was at least 15 cmH_2O higher than the baseline without expulsion of urine. BP was defined as the lowest BP during filling, MP was defined as the maximum BP during the micturition cycle, MV was defined as the volume of expelled urine, and RV was defined as the volume of urine remaining following voiding. Based on prior work [8], MI was defined as the interval between micturition contractions, while BC was defined as MV + RV. Mean values were calculated from three reproducible micturition cycles with the indicated number of independent animals per group.

Histological and gene expression analyses

Epithelial denudation, mast cell infiltration, tissue fibrosis, and apoptosis were histologically assessed by performing cytokeratin immunostaining, Toluidine blue staining (8544-4125; Daejung Chemicals & Metals, Seoul, Korea), Masson's trichrome staining (Junsei Chemical, Tokyo, Japan), and TUNEL (1 684 795; Roche, Mannheim, Germany), respectively, as previously described [8, 14, 15]. GFP^+ M-MSCs in the bladder were tracked by staining samples with a rabbit polyclonal anti-GFP antibody (ab290; Abcam, Cambridge, MA, USA) or a mouse monoclonal anti-hB2M antibody (sc-80668; Santa Cruz Biotechnology, Dallas, TX, USA). Differentiation of GFP^+ cells into epithelial, stromal, endothelial, and perivascular cells was examined by staining samples with antibodies against E-cadherin (612130; clone 36; FITC-conjugated; BD Biosciences), vimentin (sc-6260; Santa Cruz Biotechnology), CD31 (sc-376764; Santa Cruz Biotechnology), and α-SMA (ab7817; Abcam), respectively. Activation of WNT signaling was assessed by staining samples with an anti-β-catenin antibody (sc-7199; Santa Cruz Biotechnology). Alexa Fluor 488-conjugated (A11001) or Alexa Fluor 564-conjugated (A11010) anti-mouse or anti-rabbit antibodies were used as secondary antibodies (Molecular Probes, Grand Island, NY, USA). Nuclei were counterstained with 4′,6-diamino-2-phenylindole (DAPI; D9542; Sigma-Aldrich). Three representative areas per slide were randomly selected for five independent animals. Quantitative digital image analysis was performed using Image Pro 5.0 software (Media-Cybernetics, Rockville, MD, USA).

Total RNA was prepared using a RNeasy Mini Kit (Qiagen Inc., Valencia, CA). Reverse transcription was performed using TaqMan Reverse Transcription Reagents (Applied Biosystems, Foster City, CA, USA). The indicated transcripts were quantified by real-time quantitative PCR (RQ-PCR) using the PikoReal™ Real-Time PCR System (Thermo Scientific, Foster City, CA, USA) and iQ™ SYBR Green PCR Master Mix (Bio-Rad, Hercules, CA, USA), as described previously [50, 51]. Duplicate RQ-PCR assays were performed for five independent animals.

Statistical analysis

Data are reported as the mean ± standard error of the mean (SEM) and were analyzed using GraphPad Prism 6.0 software (GraphPad Software, La Jolla, CA). Differences and significance were verified by a one-way or two-way ANOVA followed by the

Bonferroni post-hoc test. A p-value less than 0.05 was considered statistically significant.

Abbreviations

BC: bladder capacity; BM: bone marrow; BP: bladder pressure; DAPI: 4',6-diamino-2-phenylindole; DAT: days after transplantation; GFP: green fluorescent protein; GRIN: gradient-index; hB2M: human β2 microglobin; HCl: hydrochloric acid; hESC: human embryonic stem cell; IAP: intra-abdominal pressure; IC/BPS: interstitial cystitis/bladder pain syndrome; IVP: intravesical pressure; LPS: lipopolysaccharide; MI: micturition interval; M-MSC: multipotent mesenchymal stem cell; MP: micturition pressure; MSC: mesenchymal stem cell; MV: micturition volume; NVC: non-voiding contraction; PBS: phosphate-buffered saline; PS: protamine sulfate; PSC: pluripotent stem cell; RQ-PCR: real-time quantitative PCR; RV: residual volume; SEM: standard error of the mean; Shh: sonic hedgehog; *Smo*: *Smoothened*; TUNEL: terminal deoxynucleotidyl transferase dUTP nick-end labeling; UCB: umbilical cord blood.

Acknowledgments

We thank Dr. Joon Seo Lim from the Scientific Publications Team at Asan Medical Center for his editorial assistance in preparing this manuscript. This research was supported by a grant from the Korean Health Technology R&D Project, Ministry of Health & Welfare, Republic of Korea (grant no. HI14C3365 and HI18C2391), by the Basic Science Research Program through the National Research Foundation of Korea (NRF-2018R1A2B2001392 and NRF-2017M3A9B4061890), by a NRF MRC grant funded by the Korean government (MSIP) (2018R1A5A2020732), by the Ministry of Trade, Industry & Energy (MOTIE, Korea) under the Industrial Technology Innovation Program (10080726), and by grants (2017-098) from the ASAN Institute for Life Sciences, Asan Medical Center, Seoul, Korea.

Supplementary Material

Supplementary figures and tables.
http://www.thno.org/v08p5610s1.pdf
Movie S1. http://www.thno.org/v08p5610s2.avi
Movie S2. http://www.thno.org/v08p5610s3.avi
Movie S3. http://www.thno.org/v08p5610s4.avi
Movie S4. http://www.thno.org/v08p5610s5.avi
Movie S5. http://www.thno.org/v08p5610s6.avi
Movie S6. http://www.thno.org/v08p5610s7.avi

Competing Interests

The authors have declared that no competing interest exists.

References

1. Wang D, Li LK, Dai T, Wang A, Li S. Adult Stem Cells in Vascular Remodeling. Theranostics. 2018; 8: 815-29.
2. Bianco P, Cao X, Frenette PS, Mao JJ, Robey PG, Simmons PJ, et al. The meaning, the sense and the significance: translating the science of mesenchymal stem cells into medicine. Nat Med. 2013; 19: 35-42.
3. Damien P, Allan DS. Regenerative Therapy and Immune Modulation Using Umbilical Cord Blood-Derived Cells. Biol Blood Marrow Transplant. 2015; 21: 1545-54.
4. Knaän-Shanzer S. Concise Review: The Immune Status of Mesenchymal Stem Cells and Its Relevance for Therapeutic Application. STEM CELLS. 2014; 32: 603-8.
5. Hong KS, Bae D, Choi Y, Kang SW, Moon SH, Lee HT, et al. A porous membrane-mediated isolation of mesenchymal stem cells from human embryonic stem cells. Tissue Eng Part C Methods. 2015; 21: 322-9.
6. Sheyn D, Ben-David S, Shapiro G, De Mel S, Bez M, Ornelas L, et al. Human Induced Pluripotent Stem Cells Differentiate Into Functional Mesenchymal Stem Cells and Repair Bone Defects. Stem Cells Transl Med. 2016; 5: 1447-60.
7. Kim JM, Hong KS, Song WK, Bae D, Hwang IK, Kim JS, et al. Perivascular Progenitor Cells Derived From Human Embryonic Stem Cells Exhibit Functional Characteristics of Pericytes and Improve the Retinal Vasculature in a Rodent Model of Diabetic Retinopathy. Stem Cells Transl Med. 2016; 5: 1268-76.
8. Kim A, Yu HY, Lim J, Ryu CM, Kim YH, Heo J, et al. Improved efficacy and in vivo cellular properties of human embryonic stem cell derivative in a preclinical model of bladder pain syndrome. Sci Rep. 2017; 7: 8872.
9. Jeong H, Yim HW, Park HJ, Cho Y, Hong H, Kim NJ, et al. Mesenchymal Stem Cell Therapy for Ischemic Heart Disease: Systematic Review and Meta-analysis. Int J Stem Cells. 2018; 11: 1-12.
10. Wezel F, Southgate J, Thomas DF. Regenerative medicine in urology. BJU Int. 2011; 108: 1046-65.
11. Kim A, Shin DM, Choo MS. Stem Cell Therapy for Interstitial Cystitis/Bladder Pain Syndrome. Curr Urol Rep. 2016; 17: 1.
12. Propert KJ, Schaeffer AJ, Brensinger CM, Kusek JW, Nyberg LM, Landis JR. A prospective study of interstitial cystitis: results of longitudinal followup of the interstitial cystitis data base cohort. The Interstitial Cystitis Data Base Study Group. J Urol. 2000; 163: 1434-9.
13. Oravisto KJ. Epidemiology of interstitial cystitis. Ann Chir Gynaecol Fenn. 1975; 64: 75-7.
14. Song M, Lim J, Yu HY, Park J, Chun JY, Jeong J, et al. Mesenchymal Stem Cell Therapy Alleviates Interstitial Cystitis by Activating Wnt Signaling Pathway. Stem Cells Dev. 2015; 24: 1648-57.
15. Kim A, Yu HY, Heo J, Song M, Shin JH, Lim J, et al. Mesenchymal stem cells protect against the tissue fibrosis of ketamine-induced cystitis in rat bladder. Sci Rep. 2016; 6: 30881.
16. Maltais S, Tremblay JP, Perrault LP, Ly HQ. The paracrine effect: pivotal mechanism in cell-based cardiac repair. J Cardiovasc Transl Res. 2010; 3: 652-62.
17. Gharaibeh B, Lavasani M, Cummins J, Huard J. Terminal differentiation is not a major determinant for the success of stem cell therapy - cross-talk between muscle-derived stem cells and host cells. Stem Cell Res Ther. 2011; 2: 31.
18. Kim JK, Lee WM, Kim P, Choi M, Jung K, Kim S, et al. Fabrication and operation of GRIN probes for in vivo fluorescence cellular imaging of internal organs in small animals. Nat Protoc. 2012; 7: 1456-69.
19. Stein PC, Pham H, Ito T, Parsons CL. Bladder injury model induced in rats by exposure to protamine sulfate followed by bacterial endotoxin. J Urol. 1996; 155: 1133-8.
20. Birder L, Andersson K-E. Animal Modelling of Interstitial Cystitis/Bladder Pain Syndrome. Int Neurourol J. 2018; 22: S3-9.
21. Lilly JD, Parsons CL. Bladder surface glycosaminoglycans is a human epithelial permeability barrier. Surgery, gynecology & obstetrics. 1990; 171: 493-6.
22. Shie JH, Kuo HC. Higher levels of cell apoptosis and abnormal E-cadherin expression in the urothelium are associated with inflammation in patients with interstitial cystitis/painful bladder syndrome. BJU Int. 2011; 108: E136-41.
23. Logadottir Y, Delbro D, Fall M, Gjertsson I, Jirholt P, Lindholm C, et al. Cytokine expression in patients with bladder pain syndrome/interstitial cystitis ESSIC type 3C. J Urol. 2014; 192: 1564-8.
24. Sant GR, Kempuraj D, Marchand JE, Theoharides TC. The mast cell in interstitial cystitis: role in pathophysiology and pathogenesis. Urology. 2007; 69: 34-40.
25. Dihlmann S, Siermann A, von Knebel Doeberitz M. The nonsteroidal anti-inflammatory drugs aspirin and indomethacin attenuate beta-catenin/TCF-4 signaling. Oncogene. 2001; 20: 645-53.
26. van der Poel HG. Smart drugs in prostate cancer. Eur Urol. 2004; 45: 1-17.
27. Chancellor MB, Yoshimura N. Treatment of interstitial cystitis. Urology. 2004; 63: 85-92.
28. Baker SC, Shabir S, Georgopoulos NT, Southgate J. Ketamine-Induced Apoptosis in Normal Human Urothelial Cells: A Direct, N-Methyl-d-Aspartate Receptor-Independent Pathway Characterized by Mitochondrial Stress. The American journal of pathology. 2016; 186: 1267-77.

29. Clemens JQ, Link CL, Eggers PW, Kusek JW, Nyberg LM, Jr., McKinlay JB, et al. Prevalence of painful bladder symptoms and effect on quality of life in black, Hispanic and white men and women. J Urol. 2007; 177: 1390-4.
30. Nickel JC, Tripp DA, Pontari M, Moldwin R, Mayer R, Carr LK, et al. Psychosocial phenotyping in women with interstitial cystitis/painful bladder syndrome: a case control study. J Urol. 2010; 183: 167-72.
31. Jhang JF, Birder LA, Chancellor MB, Kuo HC. Patient characteristics for different therapeutic strategies in the management ketamine cystitis. Neurourol Urodyn. 2017; 36: 687-91.
32. Meng E, Hsu YC, Chuang YC. Advances in intravesical therapy for bladder pain syndrome (BPS)/interstitial cystitis (IC). Lower urinary tract symptoms. 2018; 10: 3-11.
33. Mullins C, Bavendam T, Kirkali Z, Kusek JW. Novel research approaches for interstitial cystitis/bladder pain syndrome: thinking beyond the bladder. Transl Androl Urol. 2015; 4: 524-33.
34. Belknap S, Blalock E, Erickson D. The Challenges of Interstitial Cystitis: Current Status and Future Prospects. Drugs. 2015; 75: 2057-63.
35. Maeda D, Akiyama Y, Morikawa T, Kunita A, Ota Y, Katoh H, et al. Hunner-Type (Classic) Interstitial Cystitis: A Distinct Inflammatory Disorder Characterized by Pancystitis, with Frequent Expansion of Clonal B-Cells and Epithelial Denudation. PLoS One. 2015; 10: e0143316.
36. Kim A, Hoe K-O, Shin JH, Choo M-S. Evaluation of the incidence and risk factors associated with persistent frequency in interstitial cystitis/bladder pain syndrome and the efficacy of antimuscarinic treatment. Investig Clin Urol. 2017; 58: 353-8.
37. Liang X, Ding Y, Zhang Y, Tse HF, Lian Q. Paracrine mechanisms of mesenchymal stem cell-based therapy: current status and perspectives. Cell transplantation. 2014; 23: 1045-59.
38. Cosenza S, Toupet K, Maumus M, Luz-Crawford P, Blanc-Brude O, Jorgensen C, et al. Mesenchymal stem cells-derived exosomes are more immunosuppressive than microparticles in inflammatory arthritis. Theranostics. 2018; 8: 1399-410.
39. Vonk LA, van Dooremalen SFJ, Liv N, Klumperman J, Coffer PJ, Saris DBF, et al. Mesenchymal Stromal/stem Cell-derived Extracellular Vesicles Promote Human Cartilage Regeneration In Vitro. Theranostics. 2018; 8: 906-20.
40. Wang Y, Chen X, Cao W, Shi Y. Plasticity of mesenchymal stem cells in immunomodulation: pathological and therapeutic implications. Nat Immunol. 2014; 15: 1009-16.
41. Lee SW, Ryu C-M, Shin J-H, Choi D, Kim A, Yu HY, et al. The Therapeutic Effect of Human Embryonic Stem Cell-Derived Multipotent Mesenchymal Stem Cells on Chemical-Induced Cystitis in Rats. Int Neurourol J. 2018; 22: S34-45.
42. Zhang C, Murphy SV, Atala A. Regenerative medicine in urology. Seminars in pediatric surgery. 2014; 23: 106-11.
43. Sadri-Ardekani H, Atala A. Regenerative medicine for the treatment of reproductive system disorders: current and potential options. Advanced drug delivery reviews. 2015; 82-83: 145-52.
44. Cho SJ, Kim SY, Jeong HC, Cheong H, Kim D, Park SJ, et al. Repair of Ischemic Injury by Pluripotent Stem Cell Based Cell Therapy without Teratoma through Selective Photosensitivity. Stem Cell Reports. 2015; 5: 1067-80.
45. Kumamaru H, Ohkawa Y, Saiwai H, Yamada H, Kubota K, Kobayakawa K, et al. Direct isolation and RNA-seq reveal environment-dependent properties of engrafted neural stem/progenitor cells. Nat Commun. 2012; 3: 1140.
46. Song M, Heo J, Chun JY, Bae HS, Kang JW, Kang H, et al. The paracrine effects of mesenchymal stem cells stimulate the regeneration capacity of endogenous stem cells in the repair of a bladder-outlet-obstruction-induced overactive bladder. Stem Cells Dev. 2014; 23: 654-63.
47. Kim Y, Jin HJ, Heo J, Ju H, Lee HY, Kim S, et al. Small hypoxia-primed mesenchymal stem cells attenuate graft-versus-host disease. Leukemia. 2018; [Epub ahead of print].
48. Lee T, Yoon SM. The Role of Intra-abdominal Pressure Measurement in Awake Rat Cystometry. Int Neurourol J. 2013; 17: 44-7.
49. Jin LH, Shin HY, Kwon YH, Park CS, Yoon SM, Lee T. Urodynamic findings in an awake chemical cystitis rat model observed by simultaneous registrations of intravesical and intraabdominal pressures. Int Neurourol J. 2010; 14: 54-60.
50. Jeong EM, Yoon JH, Lim J, Shin JW, Cho AY, Heo J, et al. Real-Time Monitoring of Glutathione in Living Cells Reveals that High Glutathione Levels Are Required to Maintain Stem Cell Function. Stem Cell Reports. 2018; 10: 600-14.
51. Heo J, Lim J, Lee S, Jeong J, Kang H, Kim Y, et al. Sirt1 Regulates DNA Methylation and Differentiation Potential of Embryonic Stem Cells by Antagonizing Dnmt3l. Cell reports. 2017; 18: 1930-45.